CHAPTER 4

OBSERVATIONS OF HIGHLY DISPERSED PULSAR SIGNALS

4.1 INTRODUCTION

The observations reported in the previous chapter are useful for obtaining reliable estimates of average pulse energy for all eight detected pulsars and good time-resolution pulse profiles for the low DM pulsars. However, with these observations, it is not possible to obtain high time-resolution profiles for high DM pulsars. Therefore, some kind of dedispersion scheme needs to be considered. In this chapter, we describe a scheme devised to enable high time-resolution observations of high DM pulsars. In the first section, the basic scheme is presented. The hardware built and used for this purpose is described in detail. A new scheme for gain calibration, the procedures used for observation, data processing, and detection are also discussed.

4.2 BASIC SCHEME : SWEPT-FREQUENCY DEDISPERSION

For high DM pulsars, the dispersion smearing of pulsar signals becomes serious at low radio frequencies. In such cases, the time-resolution can be improved by using some suitable scheme for dedispersion of the pulsar signals. Many variations of the predetection and the post-detection dispersion removal techniques have been used at high radio frequencies (e.g.[48,27]) . The scheme employed by us involves a basic swept-frequency dedispersion procedure similar to that used by Sutton et al. (1970)[59]. In this scheme, the periodicity and the dispersed nature of the pulsar signals are used to our advantage.

The dispersion in the interstellar medium is described by the dispersion relation (see Appendix II; eq. II.4). It can be shown, that due to this dispersion the pulsar signal at any instant in time gets mapped into the frequency. domain. Therefore, a pulse profile over one full period could be obtained, if the intensity as a function of frequency can be measured over a finite bandwidth (Δf) given by (ref. Fig. 4.1),

$$\Delta f \simeq k_o P f_o^3 / DM \qquad .....(4.1)$$

assuming $\Delta f \ll f_o$

where k_o = constant

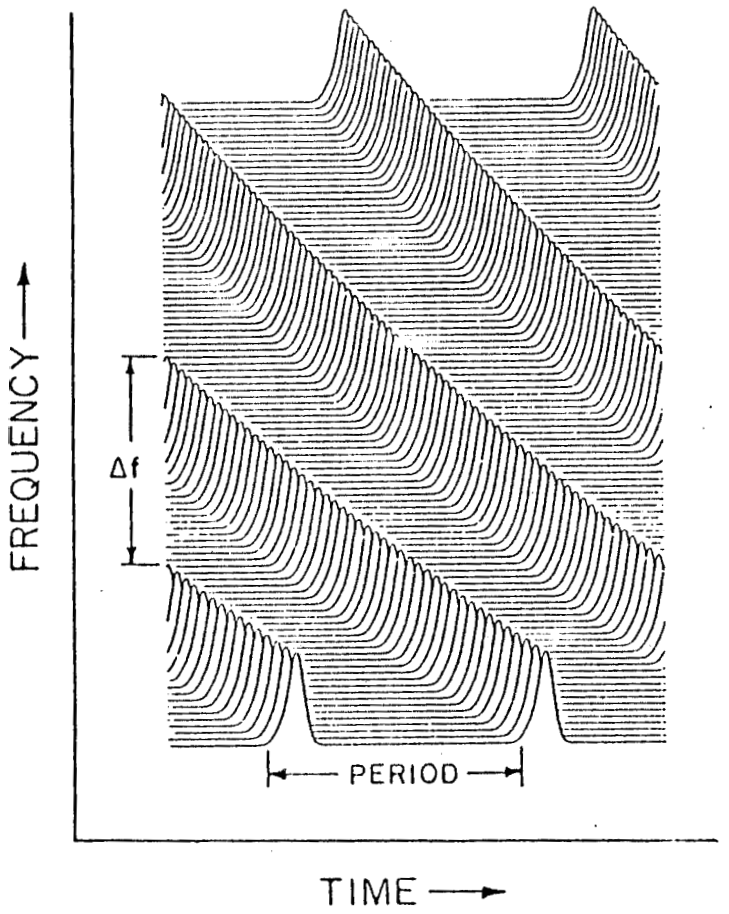

FIG. 4.1 Time to frequency mapping of dispersed pulsar signals.

f_o = centre frequency of observation

DM = Dispersion Measure

P = Period of the pulsar.

However, this intensity pattern at a later time would have shifted relative to that at an earlier time. In fact, the intensity pattern sweeps across the band at an approximate rate of $(-\Delta f/P)$. This intensity pattern can be made to appear stationary in the frequency domain by appropriately also "sweeping" the centre frequency of the receiver. Then the dispersed pulsar signal would result in a train of "fixed" spectral features separated by Af at all times. These spectral features correspond to the dedispersed pulse profiles. These intensity patterns can be now measured with high spectral resolution using a suitable spectral' line receiver. The centre frequency of observation should be swept at the rate given by the dispersion relation. The sweep can be reset at intervals of integral number of periods. The maximum time-resolution obtainable this way corresponds to the dispersion smearing occuring over the width of one spectral bin. This forms the basis of the scheme employed by us to dedisperse the highly dispersed pulsar signals and to enable observations with high time-resolution.

The existing 128 channel autocorrelation receiver was employed to enable intensity measurements in the frequency domain with high resolution. This receiver has been described in Section 2.2.2. With a suitable choice of the baseband filter and appropriate sampling clock rate, the observing bandwidth (B) can be selected. Then the spectral resolution obtainable is equal to (B/256). A maximum sampling rate of 2 MHz is possible for this receiver.

For the implementation of the above scheme (Fig. 4.2), we still require a suitable sweeping local oscillator system. In the next section, we describe this aspect in great detail.

•

4.3 THE SWEEPING LOCAL OSCILLATOR SYSTEM (SLOS)

4.3.1 Design Considerations

Let us first note our requirements that the sweeping local oscillator system should satisfy. We note from Eq. (4.1) that the bandwidth (Δf) to be swept by SLOS is a function of the dispersion measure (DM) and the period (P) of the pulsar to be observed. We have considered most of the pulsars detected at 102 MHz [63], as possible candidates for detection at 34.5 MHz, and have indicated them on the Period Vs. DM plot (Fig. 4.3). The different curves corresponding to different values of maximum bandwidth that can be swept by SLOS are indicated. It should be noted, that for a given

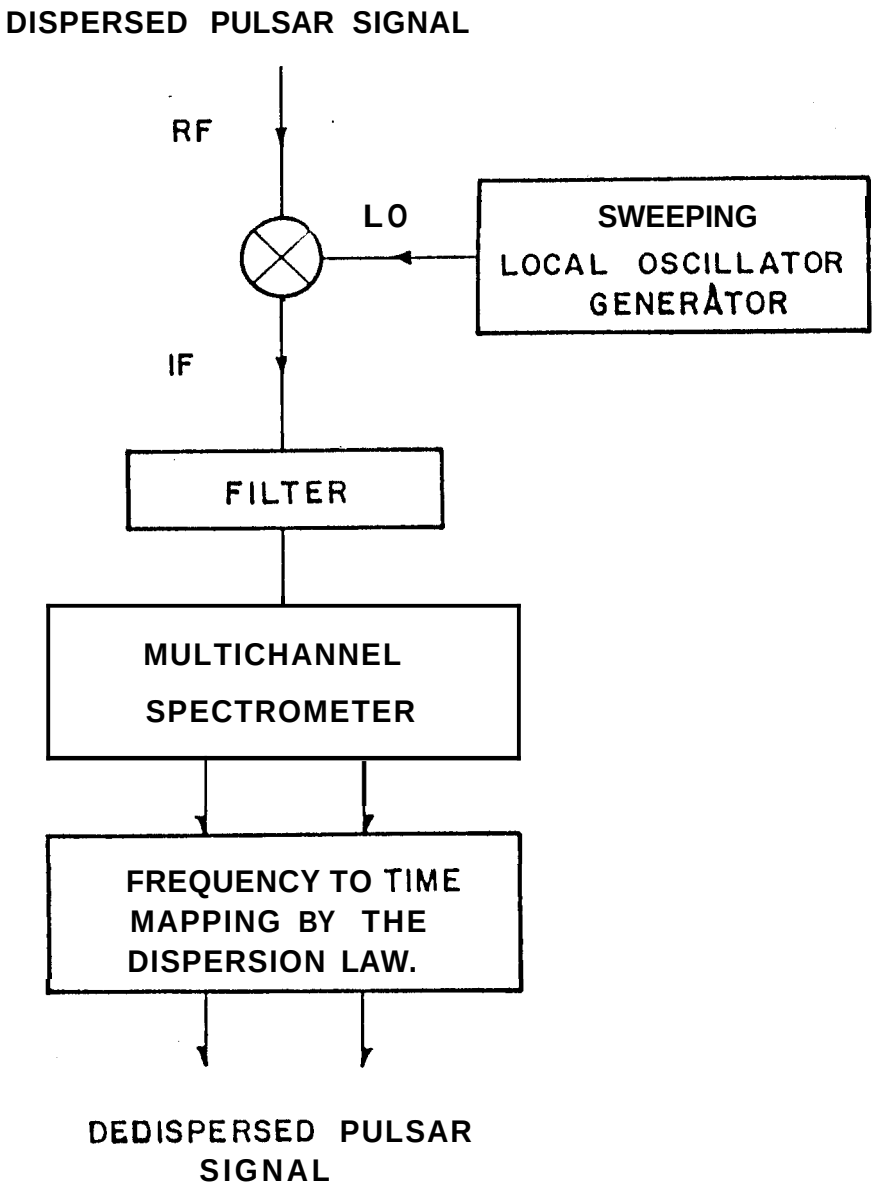

FIG. 4.2 The swept_frequency dedispersion scheme

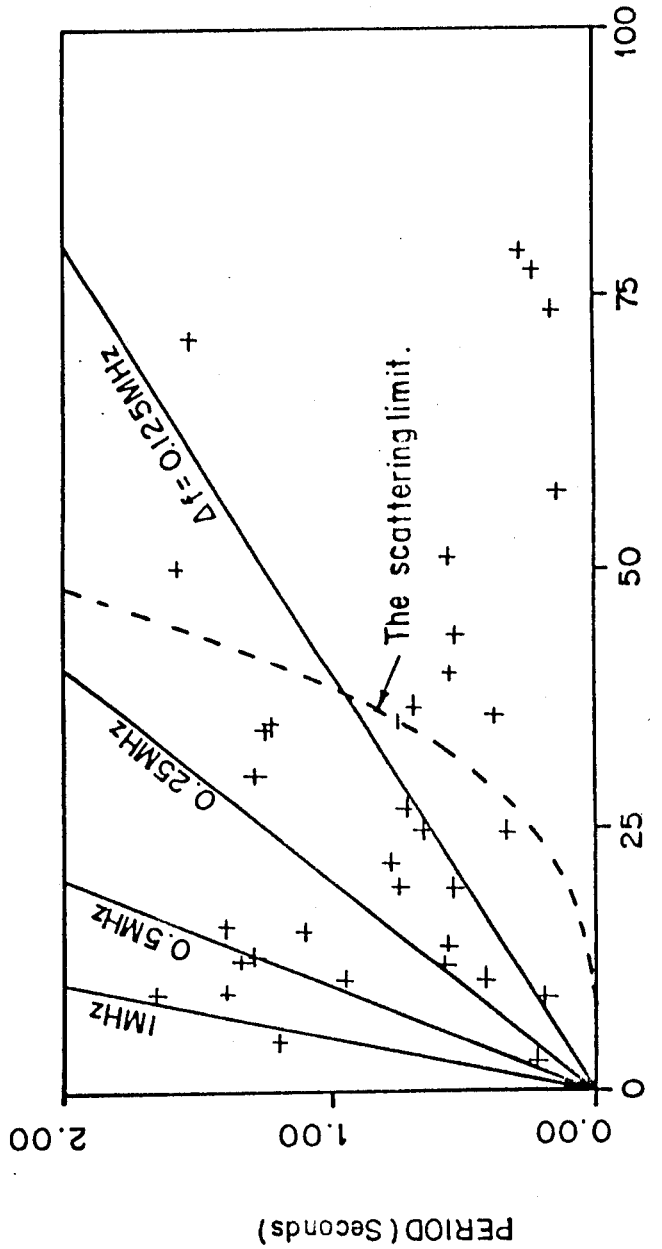

FIG. 4.3 A plot of pulsar periods Vs DMs

value of the maximum bandwidth swept by SLOS, the system can cater to observations of all pulsars indicated below the corresponding straight line. The dotted curve shows the limit set by the scattering in the interstellar medium. A pulsar which lies below this curve would have scattering width (τ_s) larger than the pulsar period (P). This curve is obtained by extrapolating the scattering width measurements at 160 and 80 MHz [70]. We have assumed that $\tau_s \propto (\text{wavelength})^4$. Note that the value of 1 MHz for the maximum sweep bandwidth is sufficient for most of the pulsars indicated here. The pulsars, which need higher sweep bandwidths, have either very low DMs or longer periods. Therefore, the effects of despersion smearing are not very serious in their cases.

The next important requirement is that the SLOS should produce the sweep as described by the dispersion relation with minimum possible error. Any errors in the sweep frequency will result in additional smearing of the intensity pattern due to the pulsar signal. Therefore the r.m.s. error in the sweep frequency produced should be less than the spectral resolution (B/256) used. The scattering limit (Fig. 4.3) suggests a minimum Δf of about 100 KHz. Assuming the same limit for B, the highest spectral resolution is 400 Hz. This means, that in the worst case, an r.m.s. error of 400 Hz can be allowed in the sweep frequency. This r.m.s. error results in an additional smearing of about 8 milliseconds for

DM = 100 cm^{-3}pc.

Thirdly, the sweep output should be centred at the centre frequency of the operation of the telescope. With the above three considerations, we require the SLOS to have sweeping capability in the band 34-35 MHz and that the sweep produced should match a given dispersion relation within a **r.m.s.** error of less than 400 Hz. Alternatively, this requirement for the output frequency $f_{out}(t)$ can be expressed more precisely as

$$f_{out}(t) = f_{\ell}(t) + \delta f(t) \qquad \ldots.(4.2a)$$

where $f_{\ell}(t)$ = required frequency

$\delta f(t)$ = error in $f_{out}(t)$; such that

$$\langle (\delta f(t))^2 \rangle^{1/2} < 400 \text{ Hz}$$

The required frequency can be found out using eq.II.3 (Appendix II) and is given by

$$f_{\ell}(t) = f_{\ell}(t') = f_S \left[1 + \frac{f_S^2 t'}{DM.k'} \right]^{-1/2} \qquad \ldots.(4.2b)$$

where $t' = t - iP$; $i = 0,1,2,.....$

such that $0 < t' < P$

and f_s = starting frequency of the sweep in the range 34-35 MHz.

k' = a constant

Before we discuss a few possible designs for the SLOS, let us note some important factors to simplify our design considerably. Firstly, the function $f_R(t)$ has a repetition period equal to the pulsar period P (Fig. 4.4a). Secondly, if we define a time parameter t" as follows

$$t'' = t'/DM \qquad \ldots\ldots(4.3)$$

then $f_R(t'')$ is a fixed function of t" (ref. eq. 4.2b). Now, such a function $f_R(t'')$ can be approximated by a staircase function f(t") as shown in Fig. 4.4b.

The function f(t") can be expressed as

$$f(t'') = f\left((\hat{n}+0.5)\Delta t/DM\right) \qquad \ldots\ldots(4.4)$$

such that $\hat{n} = 0,1,2,\ldots\ldots(\hat{n}_{max}-1)$

and $\hat{n}\Delta t \leq (t''.DM) < (\hat{n}+1)\Delta t$

The step width, $(\Delta t/DM)$, of this function f(t") should be chosen such that the r.m.s. deviation of f(t") from $f_R(t'')$ is kept well below 400 Hz. It can be shown, using eq. 4.2b, that

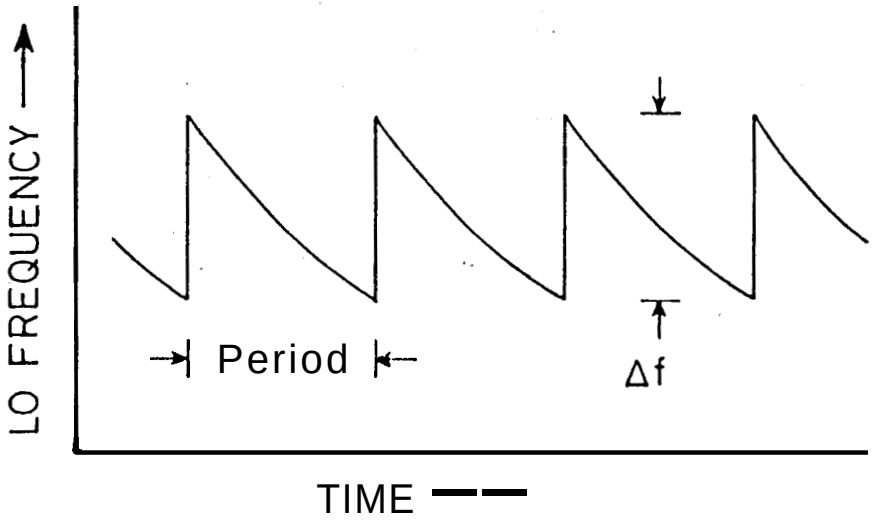

FIG. 4.4 a. The required sweep frequency $f_r(t)$

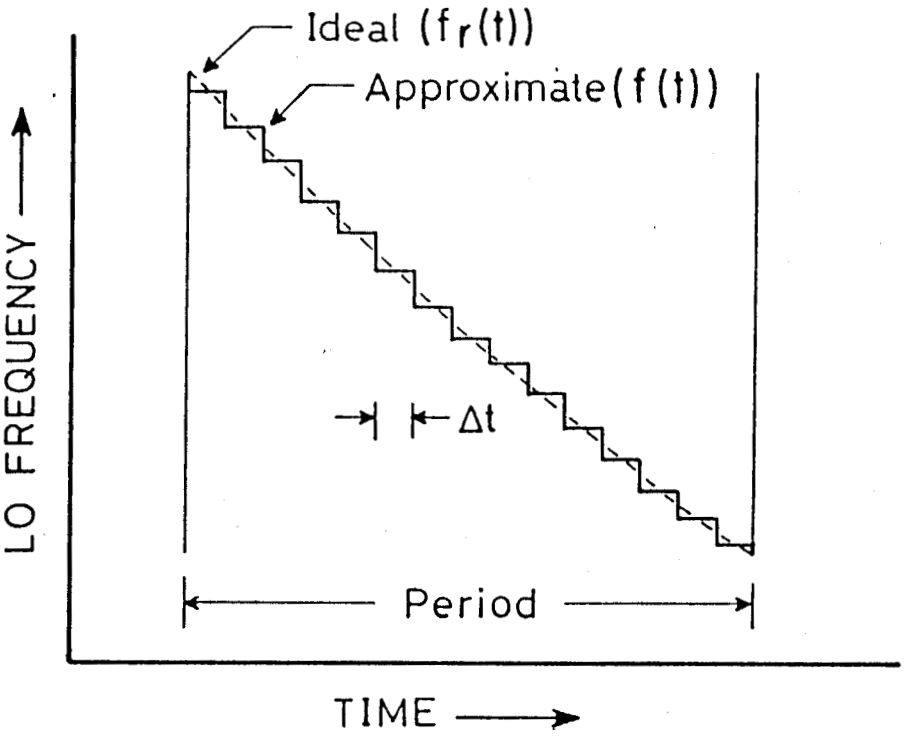

FIG. 4.4b. A Simplifying approximation for the sweep frequency.

if the step At is chosen equal to DM/20 milliseconds then the above error condition can be well satisfied. This implies that the staircase step height will be approximately **250** Hz and the number of such steps to span 1 MHz are required to be about **4000**.

Thus, if we can generate about 4000 appropriate frequencies sequentially at intervals of Δt over each period interval of the pulsar then such SLOS can satisfy our requirements. It should be noted that the accuracy of the step Δt is affected by the errors in the values of DM used. The inaccuracies in Δt cause an effective error in the SLOS output frequencies. If the value of DM can be set to an accuracy of ± 0.005 $cm^{-3}pc$, such errors can be shown to have an **r.m.s.** value of less than **250** Hz even in the worst case. Therefore, the DM value should be used to the above said accuracy. Most DM values are available to that accuracy in the literature.

Using these simplifications, we present a basic design for an acceptable SLOS as shown in Fig. 4.5. It consists of two subsystems, namely, the sweep controller and the controlled oscillator. The sweep controller, which acts as the time keeper in this case, is a programmable unit. The inputs to this unit are the values for the required starting frequency (f_S), dispersion measure (DM) and the period (P) of the ,pulsar. This unit also needs a standard time reference

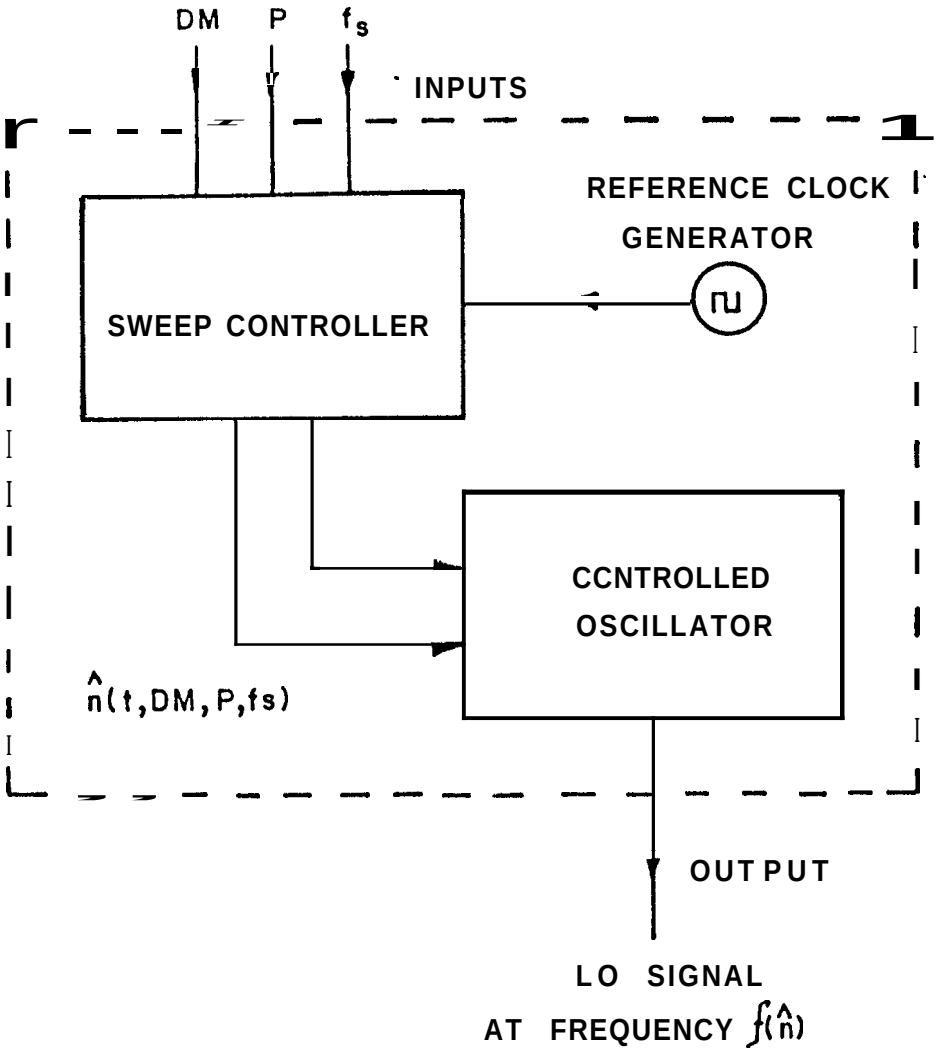

FIG. 4.5 A basic design for the SLOS.

input. Using these inputs this unit produces a sequence of values of $\hat{n}$ (ref. eq. 4.4), such that the sequence always starts with the value of $\hat{n}(=\hat{n}_s)$ corresponding to the start frequency and repeats after each interval of P seconds. The value of $\hat{n}$ is incremented by one after each time $\Delta t(=DM/20$ msec) during each block of P sec. The value of $\hat{n}$ is the input to the controlled oscillator which is required to produce a local oscillator signal with frequency given by $f_{\ell}((\hat{n}+0.5)\Delta t/DM)$ in the range 34 to 35 MHz.

4.3.2 Sweep Controller

The detail design of the sweep controller is comparatively straightforward and is shown in Fig. 4.6.

We have chosen a 1MHz standard oscillator input, as the time reference, which is adequate for the required accurracy in time-keeping. The dispersion measure value accurate to ± 0.005 $cm^{-3}pc$ can be set through a set of 4 BCD thumbwheels. Using this value and a 'rate generator' counter chain, pulses at intervals of DM/20 milliseconds are produced as shown in Fig. 4.6. These pulses are used to increment the value of $\hat{n}$ on a 12-bit binary counter. The 1MHz standard is also used to produce reset pulses at regular intervals of the period set to the last microsecond. As we will discuss later in this chapter, the reset pulses are not required to be absolutely synchronized to the arrival times of main pulses of the pulsar

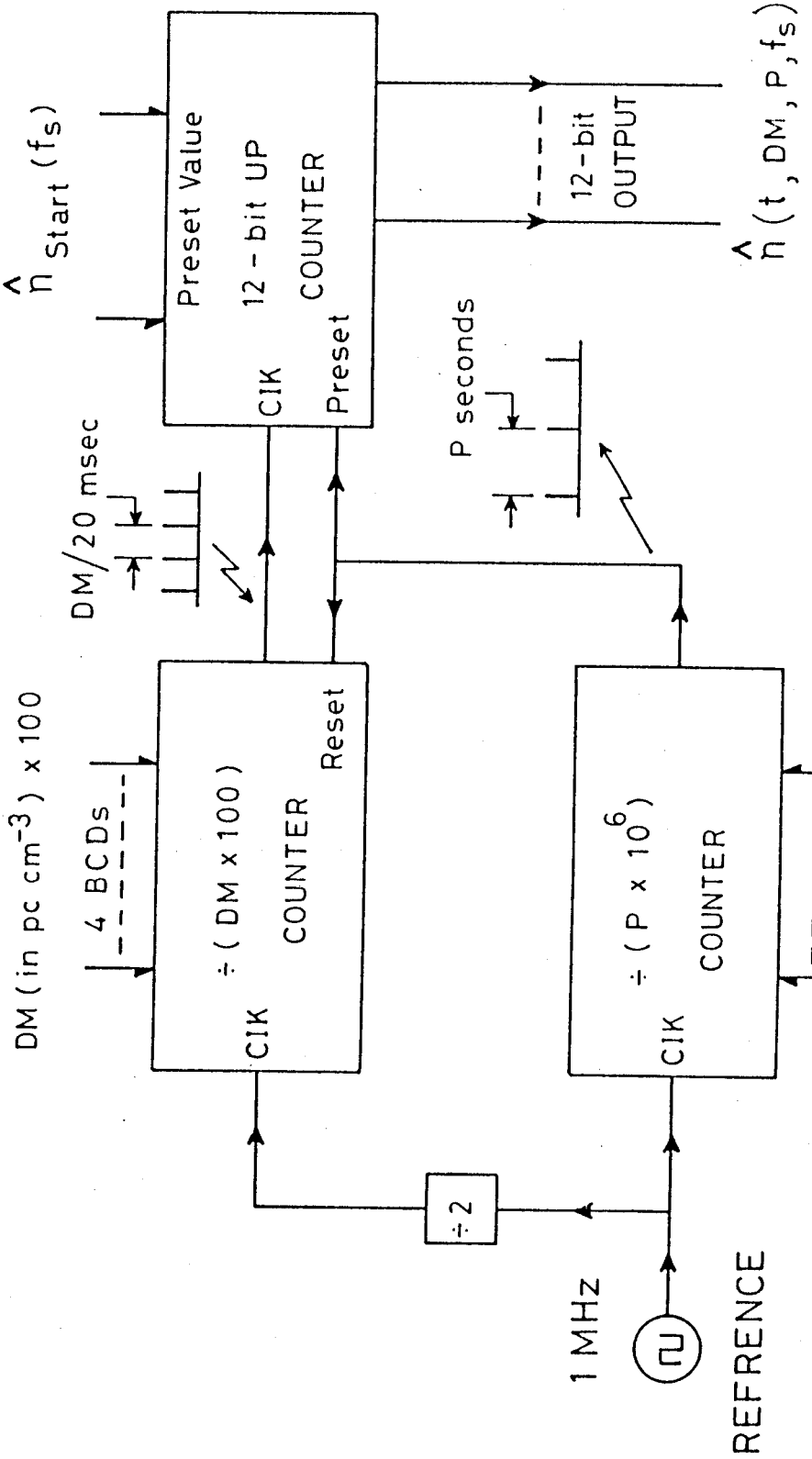

FIG. 4.6 Design of the sweep controller

signal. These reset pulses are used to reset the 'rate generator' counters as well as to preset the 12-bit binary counter to the value of $\hat{n}_s$. The value of $\hat{n}_s$ is set in steps of only about 200, which corresponds to steps of 50 KHz in f_s, which is adequate for the present purpose. This unit is realized in hardware using TTL integrated circuits.

4.3.3 Controlled Oscillator

The required controlled oscillator should be able to generate appropriate local oscillator signal depending on the value of $\hat{n}$, which can have about 4000 different values. The values of the frequencies generated should not have an r.m.s. deviation larger than 250 Hz from $f_l((\hat{n}+0.5)\Delta t/DM)$.

The most attractive possibility for this purpose, is the use of a readymade fast-switching frequency synthesiser, which can be controlled digitally. Due to the nonavailability of such an instrument for immediate use, we have considered some other possiblities.

One such design is shown in Fig. 4.7. Here, the digital representation of $\hat{n}$ is used to address a proprogrammed memory to obtain in turn a 16-bit number. This number is Digital-to-Analog converted (DAC) to produce a control voltage which is fed to a voltage controlled oscillator (VCO) to produce the frequency f_{out}. The most undesirable aspect of

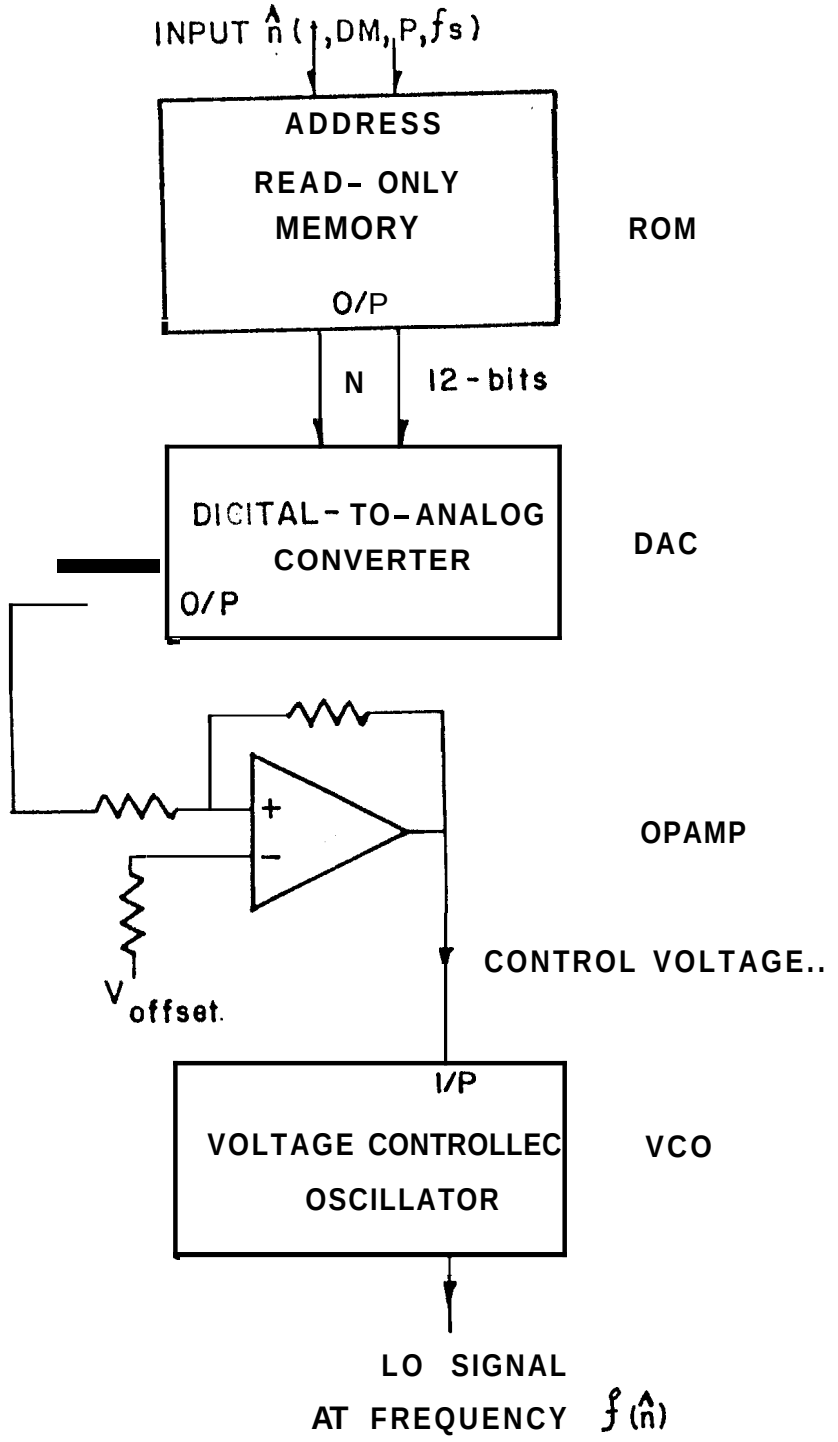

FIG. 4.7 A Design for the controlled oscillator using a DAC and a VOC.

this design is the possibility of undue drifts in the output frequencies mainly due to the temperature dependence of the VCO characteristic, the variation in the DAC reference voltage and also the gain variation of the amplifier before the VCO. It is possible to monitor the number of zero crosses of the VCO output over each period and use this number to correct the input voltage to VCO. But this can correct only a DC change in frequency and not the errors in the sweep pattern. Even otherwise, the correction can be made only after a faulty sweep is over.

Another scheme, which forms the basis of the final design adopted by us, is as shown in Fig. 4.8. The idealized scheme uses a stable frequency source at a frequency f_{in} and produces the output frequencies as close to the required ones after one stage of single side band mixing, by choosing appropriate divisor values(N). These values of N can be stored in a preprogrammed memory, addressed by the value of $\hat{n}$. This design is simple and its performance is not sensitive to voltage and temperature variations. However, there are many difficulties with this design. Firstly, it can be shown that the minimum value of f_{in} barely suitable for our purpose is given by

$$\frac{(f_{in})_{min}}{(N_{min})} - \frac{(f_{in})_{min}}{(N_{min}+1)} = 250 \text{ Hz} \qquad .....(4.5)$$

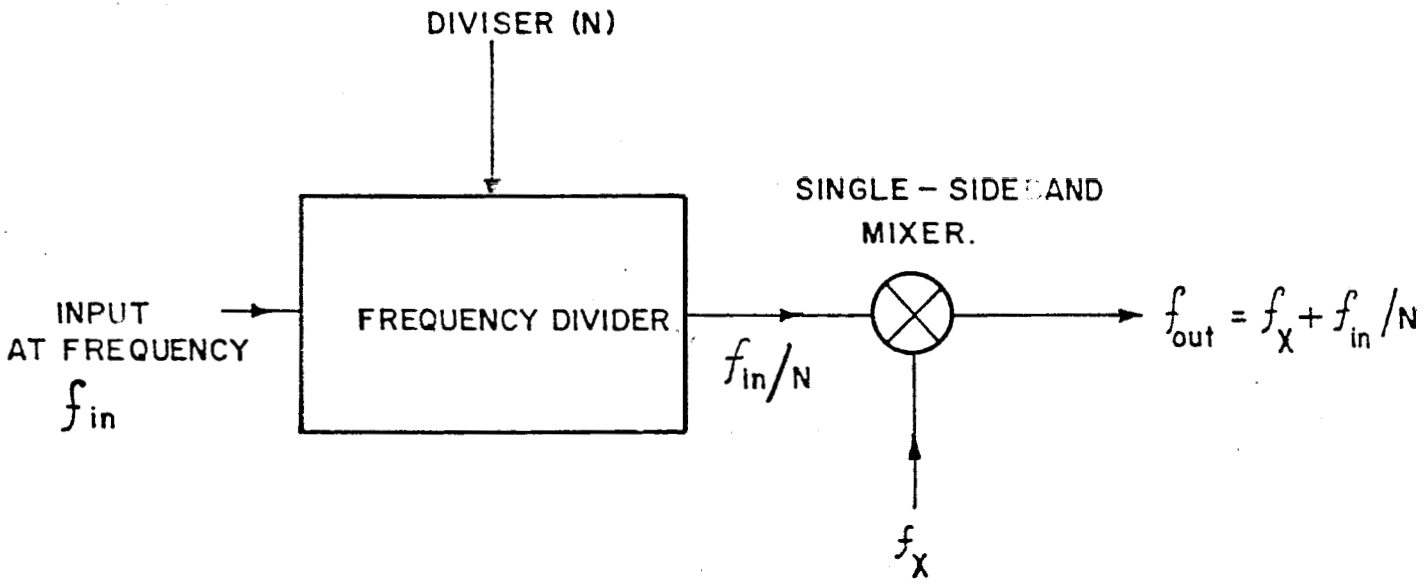

FIG 4.8 The basic divide-and-add scheme for a controlled oscillator.

This implies that for large Nmin,

$$(f_{in})_{min} \simeq 250.N_{min}^2 \text{ Hz} \qquad .....(4.6)$$

We also require a total span of 1 MHz, i.e.

$$\frac{(f_{in})_{min}}{N_{min}} > 1 \text{ MHz} \qquad .....(4.7)$$

Combining Eqs. 4.6 and 4.7 we find

$$(f_{in})_{min} > 4 \text{ GHz} \qquad .....(4.8)$$

Design of such a high frequency programmable divider is extremely difficult. Secondly, due to the digital nature of the divider output, the harmonics are impossible to supress unless the maximum value of N is reduced considerably. But this can be done only at the cost of increasing the frequency f_{in}. Therefore, this scheme using a single divider stage also turns out to be impractical. However, the basic advantages of the above scheme can be exploited, if one compromises on the number of stages that should be used. Fig. 4.9 shows a simplified block diagram for the scheme employed by us to resolve this problem. This scheme uses a 4-stage divide-and-add algorithm. The output frequency, f_{out}, given by

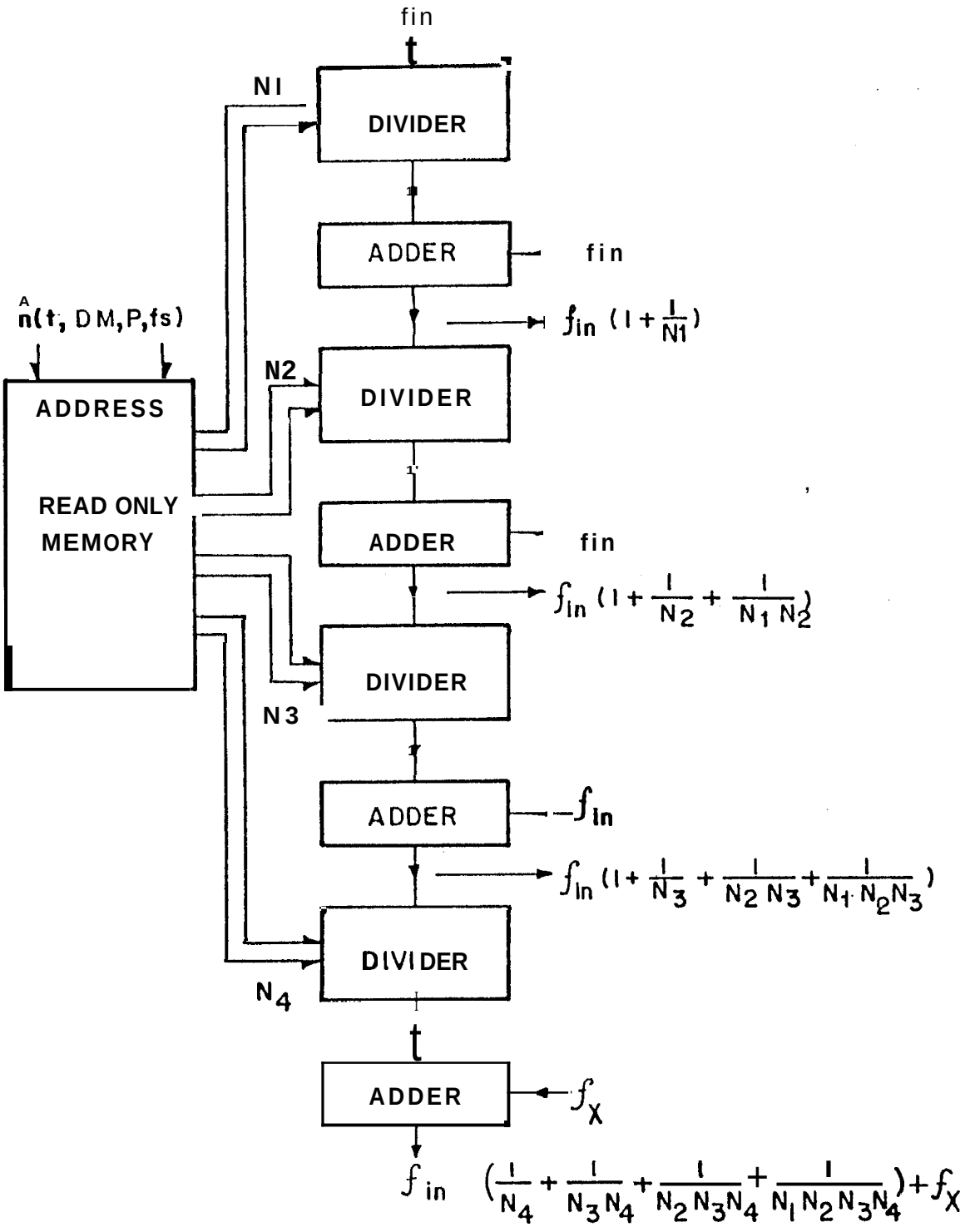

FIG. 4.9 A four stage divide-and-add scheme for the controlled oscillator.

$$f_{out} = f_{in} \left[\sum_{i=1}^{4} 1/ \left(\prod_{j=i}^{4} Nj \right) \right] + f_x \qquad .....(4.9)$$

can be generated with suitable choices of fixed frequencies f_{in} and f_x and with appropriate Nj(j=1 to 4) values. The smallest frequency f_{min} and the largest freqeuncy f_{max} that can be generated, correspond to Nj=Nmax and Nmin respectively. It should be noted'that the range of the output frequencies, i.e. $(f_{max} - f_{min})$, is directly proportional to f_{in}. With this background, we will consider some important design constrains one by one.

i) The range $(f_{max} - f_{min})$ should be at least equal to 1 MHz.

ii) Errors in the generated frequencies should be as small as possible.

iii) The adding modules will involve a mixer and a filter to pass the upper side band. The filter should be easy to realize. Therefore, Nmax, which decides the separation between the two side bands, should not be too large.

iv) The values of f_{in}, Nmax and Nmin should be such that the mixer output in the first 3 stages should not have any harmonic cotributions in the range 34 to 35 MHz.

v) The maximum frequency at which the required digital circuits may have to work should be kept well within the operating frequencies of available devices.

These constrains can be optimally satisfied if Nmax=15, Nmin=5, f_{in} =13.5 MHz and f_x = 33.023 MHz. With these parameters fixed, we require suitable designs for the programmable divider and the adder modules.

Fig 4.10 shows a block diagram for the programmable divider designed by us. The input to this module is generally the analog output of the adder module. So, it needs to be shaped to make it compatible with the digital circuitry that follows. This is achieved by using zero cross detectors (ZCD) with differential inputs. The analog input levels as low as -15 dBm can be satisfactorily be converted to TTL compatible swing (0 to 5 V) at the output of the ZCD. Thus, tne use of a ZCD avoids the need for a separate amplifier. The divide-by-N outputs of counters, in general, have very small duty cycles and are therefore rich in higher harmonics. Since it is essential to minimize such harmonic content at the output of this module we have to produce a square wave output at the required output frequency. For this purpose we generate a digital signal at twice the input frequency first, The frequency doubling is achieved by exclusive-oring the two ZCD outputs produced with about quarter cycle phase difference as shown in the Fig. 4.10. This signal is first divided by the

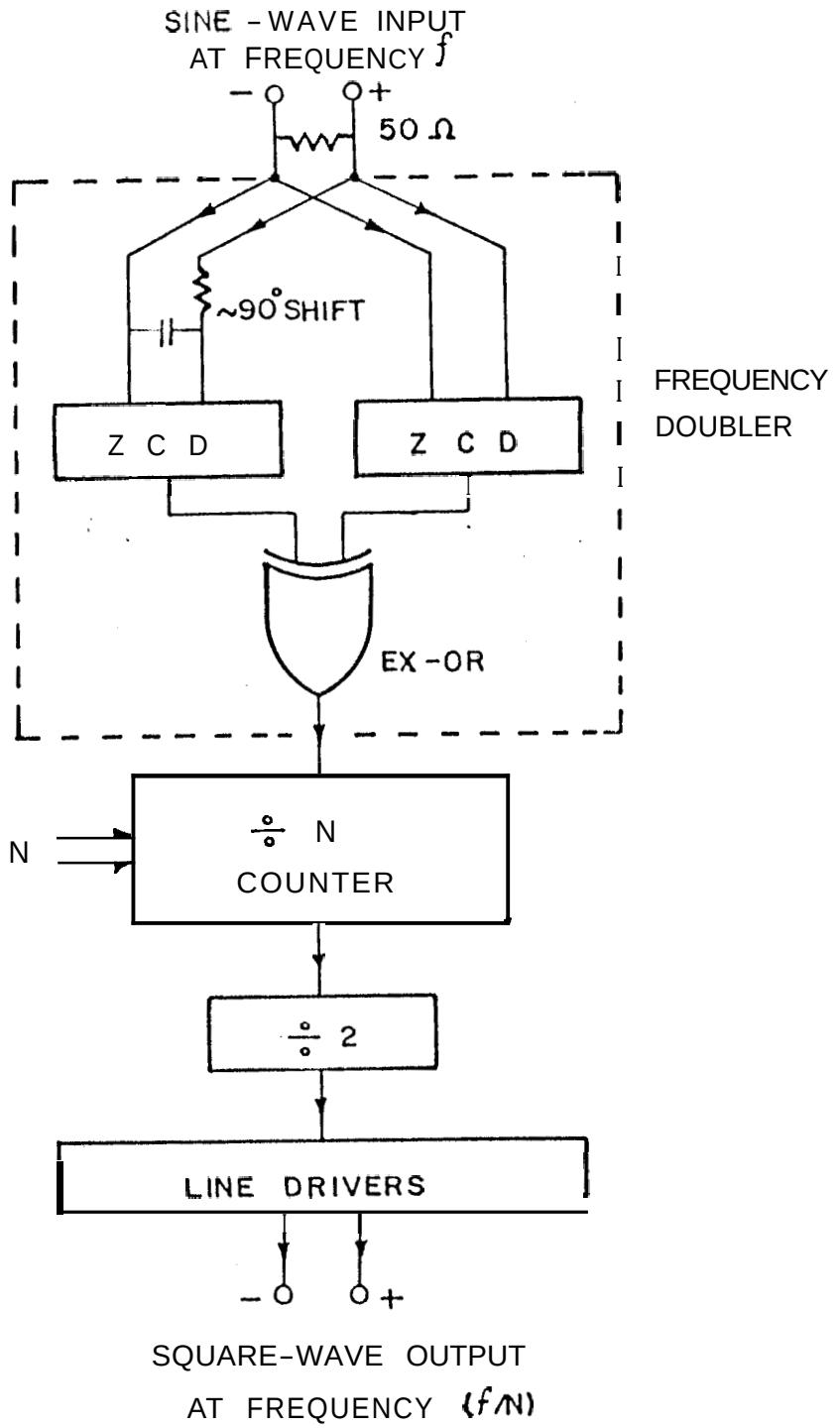

FIG. 4.10 Design of the programmable divider.

programmable divide-by-N counter, and then by a D-flipflop configured as divide-by-2 to produce a square wave at the required output frequency. The output is made available through line drivers to be able to drive the 50 ohm load of the adder module. The differential outputs of the line drivers isolate the analog and the digital grounds at the module level. This module is realized in hardwsre using suitable low power shottky and fast TTL devices.

The block diagram for the adder design is shown in Fig. 4.11. Both the HF and LO square wave inputs are AC coupled and low pass filtered to obtain only the fundamentals. Note that in an ideal square wave, the second harmonic is nonexistant. Therefore, mainly the third and higher odd harmonics are to be rejected in this low pass filtering. The RF and LO signals are then mixed using a passive mixer module and the mixer output is filtered to reject the lower side band product. Third order Tchebyshev filter characteristics are chosen to meet the requirements of the filters in the first three stages.

The output of the final adder module is passed through a ZCD and filtered for the fundamental in the range 34 to 35 MHz to give +10 dBm output level.

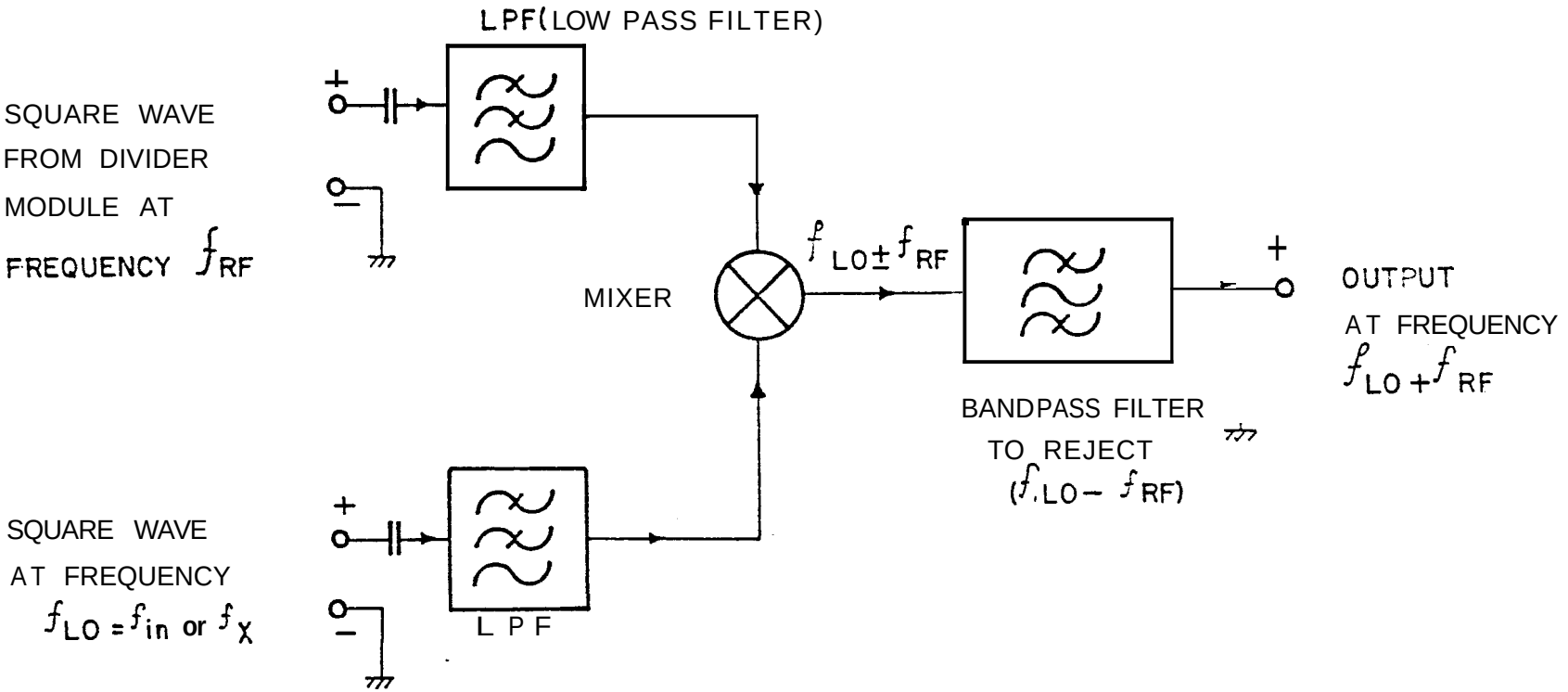

FIG. 4.11 Design of the frequency adder module.

Following the designs discussed above the controlled oscillator was built successfully. Two readily available synthesisers were used to provide the two inputs namely, f_{in} and f_{χ}.

The digital and analog modules were shielded individually. Spurious signals at the output were kept 30 dB below the main frequency output. Suitable values of Nj were made available as a function of the value of $\hat{n}$ (for $\hat{n}$=0 to 4095) in a preprogrammed memory block. The distribution of the deviation of the final output frequency from the required frequency is plotted in Fig. 4.12a,b.

Thus, the combination of the sweep controller and the controlled oscillator described here gives us a ready SLOS that can be used in the dedispersion scheme for pulsar observations with high tirne-resolution.

4.4 NEW SCHEME FOR GAIN CALIBRATION

As discussed in the beginning of this chapter, the intensity pattern in the spectral domain due to the pulsar signal can be made to appear stationary by the use of a suitable sweeping local oscillator system. Let us assume, that the SLOS frequency $f_{out}(t)$ is swept from f_s to f_e (such that $f_s > f_e$) in each interval equal to P' starting from time t=O upto time $t=t_{on}$. The average intensity pattern at the

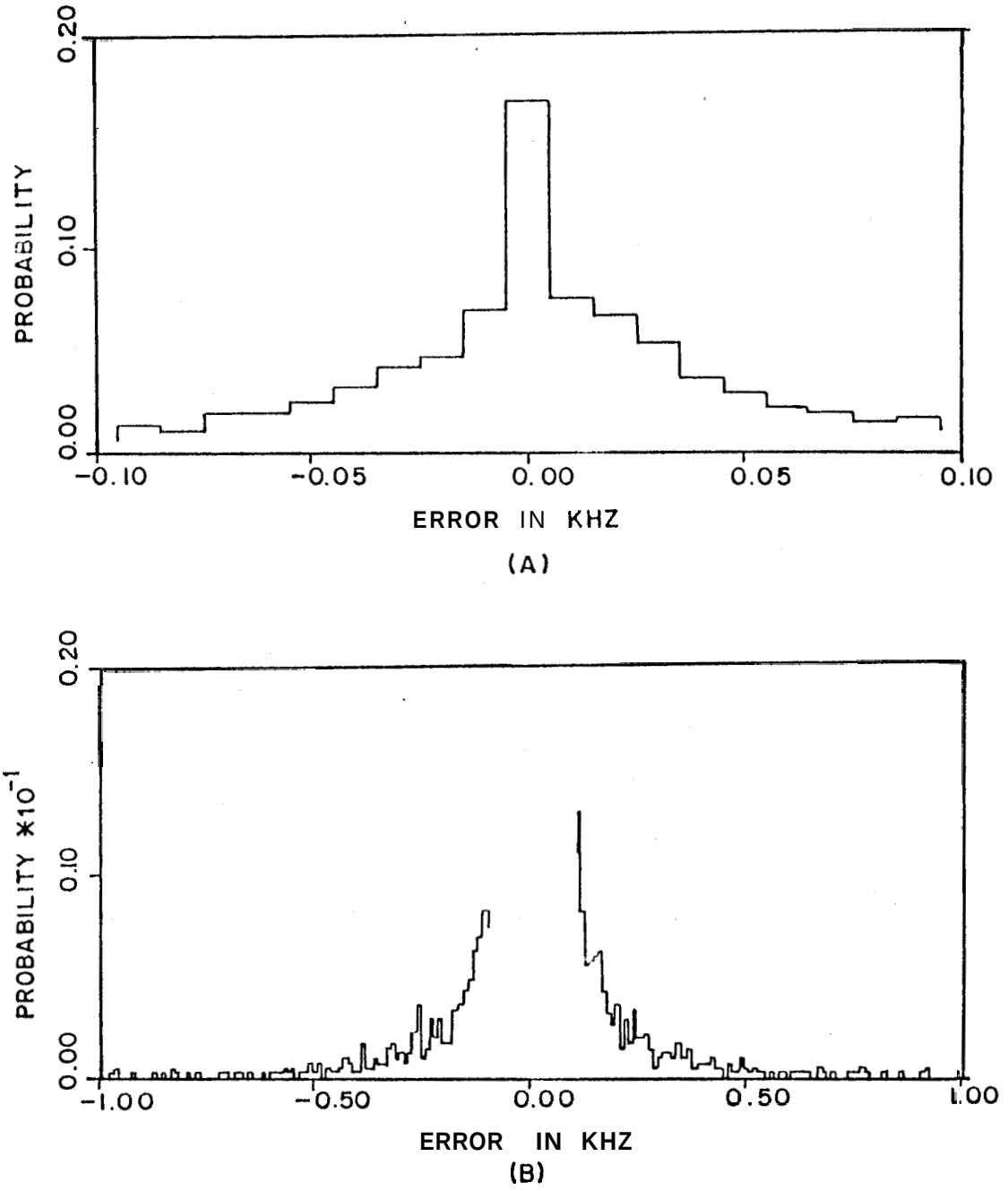

FIG. 4.12 The distribution of errors in the final output frequency of the SLOS.

output (see Fig. 4.13) can be expressed in general as

$$\bar{I}(n) = \frac{1}{t_{on}} \int_{0}^{t_{on}} \left[\frac{1}{\delta f} \int_{-\delta f/2}^{+\delta f/2} |G_a(f_{RF})|^2 \, |G_b(f_{LF})|^2 \, [Ip(f_{RF},t) + I_B(f_{RF},t)] df \right] dt \quad \ldots.(4.10)$$

where n = bin index of the output intensity pattern

δf = resolution of the spectrum/bin width

G_a = gain function of the telescope system upto the mixer stage

G_b = gain of the baseband filter

$Ip(f_{RF},t)$ = spectral density of the pulsar signal at the input of the Antenna

$I_B(f_{RF},t)$ = spectral desnity of the background radiation

$$f_{RF} = f_{out}(t) + n.\delta f + f$$

$$f_{LF} = n.\delta f + f$$

and $\delta f << f_s - f_e << f_{out}$

If the interval (P') of each sweep is equal to the apparent period (P) of the pulsar and if the duration of observation, t_{on}, is an integral multiple of P, then eq. (4.10) can be simplified as

$$\bar{I}(n) \simeq g(n) \, [\bar{I}p(\phi_s(n)) + \bar{I}_B] \quad \ldots.(4.12)$$

where,

$$g(n) = \frac{1}{P}\int_{0}^{P}\left[\frac{1}{\delta f}\int_{-\delta f/2}^{+\delta f/2}|G_a(f_{RF})|^2\,|G_b(f_{LF})|^2\,df\right]dt \qquad ....(4.13)$$

and $\bar{I}_P(\phi_s(n))$ = time average of the intensity of the pulsar signal at longitude $\phi_s(n)$

$\phi_s(n)$ = longitude of the pulsar signal at the frequency $(f_s+n\delta f)$ and at tine t=0.

$\bar{I}_B$ = time average of the intensity of the background radiation.

We have assumed, that over a small bandwidth δf, all the above functions can be considered to be constant. It should be noted, that for obtaining the intensity profile corresponding to at least one period of the pulsar signal a total bandwidth of atleast Δf (as in eq. 4.1) should be used. Further, to estimate the quantity $[\bar{I}_P(\phi_s(n))+\bar{I}_B]$, we need Lo know g(n) to great accuracy. As the quantity g(n) includes the antenna and the array component responses, it can be best measured by making observations off the source. In such a case, the measured intensities $\bar{I}_{off}(n)$ are given by

$$\bar{I}_{off}(n) \simeq g(n)\ \bar{I}'_B \qquad ....(4.14)$$

where $\bar{I}'_B$ = the background noise intensity off the source.

Thus the measured intensities can be treated as the function g(n) with a scaling factor. However, the accuracy to which g(n) can be measured, i.e. $\Delta g(n)$, is given by

$$\Delta g(n) = \frac{\Delta I_{off}(n)}{\bar{I}_{off}(n)}\, g(n) \qquad \ldots.(4.15)$$

where

$$_{off}(n) = \frac{m' \bar{I}_{off}(n)}{\sqrt{\delta f\ t_{off}}} \qquad \ldots.(4.16)$$

m' = a receiver dependent constant

and t_{off} = the duration of such an observation

The uncrrtainity in the estimation of $Ip(\phi_s(n))$ can be shown to be

$$\Delta Ip \propto \frac{\bar{I}_B}{\sqrt{\delta f}} \left[\frac{1}{t_{on}} + \frac{1}{t_{off}} \right]^{1/2} \qquad \ldots.(4.17)$$

where $\bar{I}_B$ is assumed to be equal to $\bar{I}'_B$ for simplicity.

If the off-source measurements are made by switching the beam on and off the source at a fast rate, then $t_{on} \sim t_{off}$ typically. The switching reduces the effective observing time

on the source by a factor of 2. These factors will worsen the attainable sensitivity by a factor of 2, even if we ignore the problems associated with the fast beam switching. Another way is to make such off-source observations over a separate time span. Then the uncertainity due to g(n) can be made neglegible if $t_{off} \gg t_{on}$. Thus the off source measurements need to be made over typically over 3-4 hours. Apart from such large overheads in the observing time, it is also required that g(n) does not change over the enitre interval of observation. It should be noted that the function g(n) will be different for different values of the period and the dispersion measure. These factors make such off-source measurements extremely time consuming.

Here we suggest a new scheme for gain calibration, wherein we avoid the need for an accurate estimation of the g(n). We have noted already that the spectral intensity pattern due to the pulsar signal is made to appear stationary if the appropriate LO sweep is reset only at intervals of the integral number (L_o) of the apparent period (P) of the pulsar. In our case, we will concentrate on the case when $L_o = 1$. Any deviation ΔP in such reset intervals causes the spectral intensity pattern to drift at a rate given by

$$(df/dt)_d = (\Delta P/P).(df/dt)_{SW} \qquad ....(4.18)$$

where $(df/dt)_{SW}$ = the sweep rate of the SLOS

and $\Delta P \ll P$

If the intensity pattern is averaged for a long time without accounting for such a drift the pulsar features would be smeared over the total drift. However, if the intensity patterns are sampled frequently enough and are averaged suitably by accounting for the drift, the average output intensity would have an effective gain g'(n), given by

$$g'(n) = (1/t_{on}) \int_0^{t_{on}} g(n'(t))\, dt \qquad ....(4.19)$$

where

$$n'(t) = INT\left[Frac\left[\frac{(n+n_d(t))}{(\Delta f/\delta f)} \right] .(\Delta f/\delta f) \right] \qquad ....(4.20)$$

and $n_d(t)$ = the number of bins by which the pattern drifts in time t

$$= (df/dt)_d \,.(t/\delta f)$$

It can be shown, that if

$$n_d(t_{on}) = N_d\,(\Delta f/\delta f) \qquad ....(4.21)$$

where N_d = integer number of drift cycles
= 1,2,.....

then the effective gain g'(n) will have a constant value, say $\bar{g}$, irrespective of n. This condition implies that

$$t_{on} = \frac{N_d \bar{P}}{\Delta P} \qquad \ldots.(4.22)$$

Thus, with a suitable choices of t_{on}, AP and N_d, it is possible to obtain an average intensity pattern for the pulsar signal without needing an accurate measurement of g(n). It should be pointed out at this stage, that if there exist large deviations within the gain function g(n) from its mean value, then the final signal-to-noise ratio attainable in the above scheme is reduced. In such a case, a crude estimate of g(n) can be used to divide the individual intensity patterns before averaging, so as to reduce the deviations in the effective gain function drastically. The modified gain function is given by

$$g1(n) = g(n)/g_o(n) \qquad \ldots.(4.23)$$

where $g_o(n)$ = the crude estimate of g(n)

The crude estimate $g_o(n)$ can be obtained by averaging the individual patterns without accounting for the deliberate drift $(df/dt)_d$ and be used after suitable normalization. Further, it should be noted, that the above solution is based on an assumption that the intensity pattern for the pulsar signal does not fluctuate during the observation. However, this assumption does not strictly hold good in practice. Then, the final intensity pattern would correspond to the weighted (w.r.t. gl(n)) mean intensity pattern of the pulsar signal. The final profiles would be affected most due to this problem if N_d = 1. Assuming that the fluctuations are random, this problem can be overcome to a large extent by choosing higher values of N_d . For given values of t_{on} and P, this would imply (ref. eq. 4.22) higher values of ΔP. However, any nonzero value of AP would cause additional smearing typically of the order of

$$\delta t = (\Delta P/P)\ Ts \qquad \ldots.(4.24)$$

where Ts = the sampling interval

This smearing should be as small as possible. If the sampling interval ,Ts, is comparable to P, then this condition can be stated otherwise as

$$(\Delta P/P) << (\delta f/\Delta f) \qquad \ldots.(4.25)$$

Therefore, the value of ΔP needs to be optimized with respect to N_d and δt. With a suitable choice of the above mentioned parameters, the output intensity pattern, $\bar{I}(n)$, can be expressed as

$$\bar{I}(n) \simeq \bar{g} \left(\bar{I}_p(\phi_s(n) + \bar{I}_B \right) \quad \ldots.(4.26)$$

As $\bar{I}_p \ll \bar{I}_B$, a flux calibration could be obtained almost directly if an independent estimate of $\bar{I}_B$ is available.

Apart from avoiding accurate measurements of the gain function $g(n)$ on a routine basis, the above scheme has some more interesting and important advantages. In the earlier scheme, where $\Delta P=0$, we need to observe over a bandwidth equal to or greater than Δf, to obtain the intensity pattern over one full period. It should be pointed out that the pulsar emission at low radio frequencies may not be limited to the main pulse and the interpulse window alone [78]. This aspect makes it necessary to observe the intensity pattern over at least one full period. This constraint in turn limits the resolution in time domain to P/NCH in general, where NCH is the number of spectral channels. However, our scheme readily provides a possibility of increasing the resolution beyond the above limit. In this scheme, if the observing bandwidth (B)

is chosen smaller than Δf, then the time-resolution obtainable increases by a factor $\gamma = \Delta f / B$. The observing bandwidth can be decreased upto the limit when B/NCH becomes equal to the r.m.s. error in the SLOS output frequency. However, the price for such resolution improvement is paid in terms of the reduction in the sensitivity by a factor of $\sqrt{\gamma}$. The other advantage, which is quite important but implicit in this scheme, is that of not requiring absolute synchronization of the sweep with respect to the arrival time of the main pulse in the pulsar signal.

Thus, we note that the case when $\Delta P \neq 0$, has many important advantages compared to the conventional case when $\Delta P = 0$. We have used this new scheme for the high resolution observations of pulsar signals successfully.

4.5 PROCEDURES FOR OBSERVATIONS AND DATA ACQUISITION

In this section, we describe the procedures adopted for the pulsar observations using the above discussed schemes. The basic receiver set-up is shown in Fig. 4.13.

It should be noted, that the autocorrelation receiver (ACR) can be fed with only one input signal. The antenna outputs are available from both the EW array and S array separately. The possible single inputs to ACR are namely the (E+W), S or (E+W+S). The choice of (E+W+S) is obvious for the

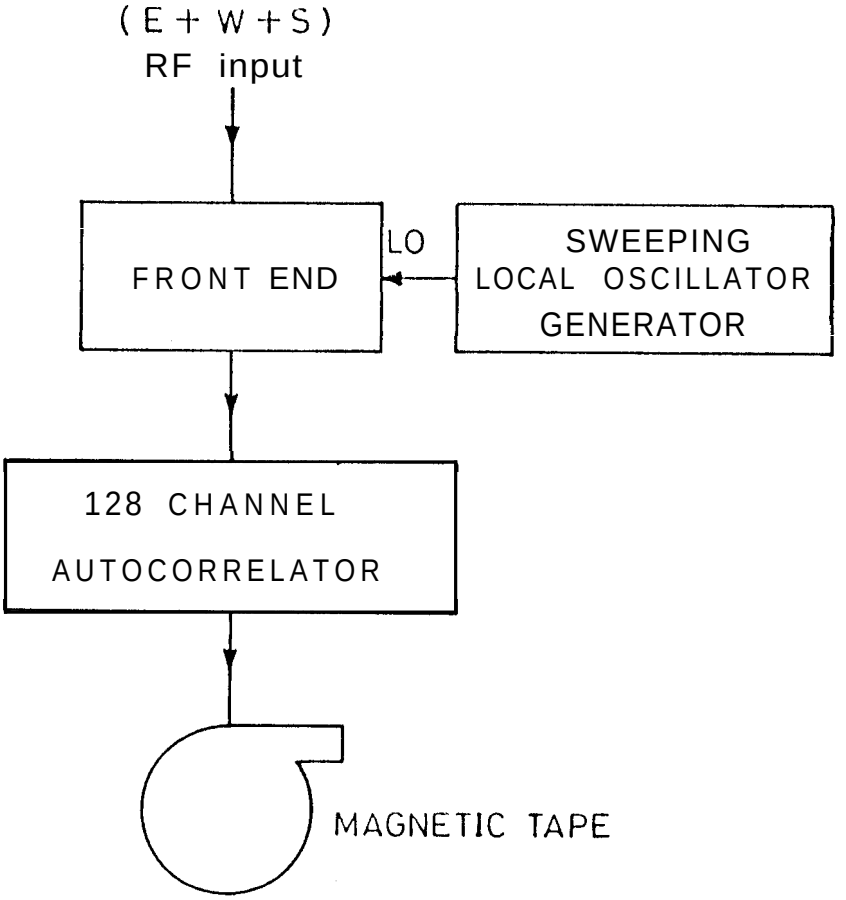

Fig. *4.13* THE BASIC RECEIVER SET-UP USED FOR OBSERVATIONS OF HIGHLY DISPERSED PULSAR SIGNALS.

ACR input, due to the high effective aperture area corresponding to it. The beam pattern corresponding to this $(E+W+S)^2$ node is quite complex, and can be split as

$$R((E+W+S)^2) = R((E+W)^2)+R(S^2)+2.R((E+W)xS) \quad ....(4.27)$$

where R("x") = the beam pattern in "**x**" mode.

The first two terms in the right hand side of the above equation correspond to two orthogonal fan beams, while the last term corresponds to a pencil beam due to the correlation. Thus the resultant beam has an effective resolution much poorer compared to that in the case of correlation. This aspect does not pose any serious problem in the case of pulsar observations, as the probability of encountering a "confusing" pulsar, with its period and DM very close to that for the pulsar of interest, in the total field of view is very small. In this mode, the tracking facility can also be used to obtain longer observing time.

The single input (E+W+S) is obtained by combining the (E+W) and S signals with equal phases. Amplitudes of the E+W and the S inputs are adjusted, such that all the basic array elements contribute equally at the combiner output.

The SLOS is used with suitable settings. The relevant value of the Dispersion Measure (DM) is set accurate to ± 0.005 $cm^{-3}pc$. The sweep reset period is set different than the apparent pulsar period, such that $(\Delta P/P) \sim 2 \times 10^{-3}$ typically. The starting frequency for the sweep is chosen suitably to centre the sweep approximately at 34.5 MHz.

Different observing bandwidths (B) can be employed by using appropriate base band filters and the sampling clock frequency. The choice of this bandwidth determines the signal-to-noise ratio and the time-resolution obtainable in the output profiles for given pulsar parameters.

The on-line integration time (τ_{on}), to average the COS and SIN correlations, can be selected in the range $(2^{12} \rightarrow 2^{19})/f_{clk}$ where f_{clk} is the sampling clock frequency. The averaged correlations available at the output of this receiver are recorded on a magnetic tape. The sampling time, Ts, is equal to the on-line integration time (τ_{on}).

In order to recover the absolute amplitude information lost due to the one-bit processing in the receiver, it is required to measure the signal power at the input of the zero cross detectors. Outputs of four threshold detectors/ integrators [87] employed for this purpose are also recorded along with the autocorrelations.

4.6 DATA PROCESSING AND DETECTION

The data recorded during these observations consists of the autocorrelation function obtained using the autacorrelation receiver-SLOS combination. Here, we describe the procedure employed for processing of such data. The autocorrelations available are normalized one-bit autocorrelations at positive delays. The processing involves the following steps.

i) **Van-vleck** Correction: The one-bit correlation values are used to compute the corresponding analog correlations through the Van-vleck relation.

$$\rho_a = \text{SIN}(\pi\rho_c/2) \qquad \ldots.(4.28)$$

where ρ_a = the normalized analog correlation

ρ_c = normalized one-bit correlation

This computation is performed for both the COS and the SIN channels.

ii) Denormalization: As already noted, the absolute amplitude information is lost in one-bit processing. However, if estimates of the total signal power at the input of the zero-cross detector is available, as in the present case, it is possible to recover the absolute amplitude information.

The available estimates of the total power are used to multiply the normalized correlations to obtain the denormalized values for autocorrelations.

iii) Power spectrum: The denormalized COS and SIN autocorrelation values obtained for positive delays are combined to get a complex Hermitian symmetric autocorrelation function. The autocorrelation function and the power spectrum of the signal form a Fourier transform pafr. We use a 256 point Fast Fourier Transform (FFT) routine [101] to fourier transform the autocorrelation function and obtain a power spectrum.

Thus, a power spectrum is obtained corresponding to each of the autocorrelation functions sampled at every interval of the on-line integration. Two power spectra are obtained in a single FFT routine call, thus reducing the time required for these computations to half. Here we make use of the fact that the power spectrum is a real function. Therefore, it is possible to combine two samples of the complex autocorrelation function linearly in an .appropriate manner, such that when fourier transformed, the real and imaginary parts of the spectrum correspond to the two required spectra.

iv) Average band shape: The power spectra obtained over the observing interval are averaged together to obtain a function representing the average gains of the spectral bins,

i.e. the gain function $g_o(n)$ of the antenna-receiver combination. It should be noted that the band shape thus obtained is not affected by the presence of pulsar signals on the average, because of the deliberate slow drift of the spectral pattern due to the pulsar signal.

v) Extraction of Pulsar signals:

Each of the power spectra contains a spectral pattern due to the observed pulsar signal. This pattern is weighted by the gain function of the receiver across the spectral band. We use the gain function $g_o(n)$ obtained earlier to divide each power spectrum so as to roughly equalize the receiver gain across the spectral pattern. The spectrum thus obtained, ideally has a dc pedestal on which the pulsar pattern buried in the background noise is placed. The value of the dc pedestal corresponds to the average power due to the background noise (P_{noise}).

Each spectrum contains 255 spectral points. Using an appropriate dispersion law, the spectral pattern is converted to a time domain pattern. .Thus, from each power spectrum 255 intensities' in the time domain are obtained. The sampling in this domain is generally nonuniform. This procedure is repeated for all power spectra obtained for regular intervals of the on-line integration. The final time series obtained over the total observing interval (t_{on}) is then processed

using a procedure similar to that described in Chapter 3. The bin-width in the time domain is chosen as close as possible to the dispersion smearing over one spectral bin, such that the apparent period is divided into integral number of bins (= NB/2). Using similar procedure as described by eq.3.4 and 3.5, the total contribution A(I) and the total number of samples C(I) added as a function of the bin number I are computed. An average profile over a two-period stretch is obtained as

$$Ave(I) = A(I)/C(I) \qquad ....(4.29)$$

where $0 \leq I \leq NB-1$

The average profile (Ave(I)) over a two-period stretch is tested for significant detection of two pulses which should be seperated by exactly one period. The threshold for significant detection is chosen to be equal to three times the r.m.s. deviations due to the noise in the two-period stretch. The value for the r.m.s. noise deviations (σ) is computed using the following equation.

$$\sigma = \frac{m' \; P_{noise}}{\sqrt{\bar{C} \; \tau_{on} \; \delta f}} \qquad ....(4.30)$$

Where $$\bar{C} = \sum_{1=1}^{NB-1} C(I)/NB \qquad ....(4.31)$$

= the mean number of samples averaged

In case of successful detection, the final average profile is obtained by combining the two halves of the corresponding two-period stretches.

vi) Baseline removal: In an ideal case, the final profile has a flat baseline corresponding to the average noise power per bin (P_{noise}). However in practice, the baselines are generally not flat. Such baselines can result from any low level broadcast interference within the observing band when swept across the band over Δf, and cannot be expected to have any systematic shape in general. Such baselines are removed in the following way. For the purpose of baseline estimation the full data in the pulse profile except that within the main pulse window is used. The data within the pulse window is replaced by the interpolated data obtained using the data on either sides of the window. The new data without the main pulse is smoothened suitably to allow only the variations broader than the pulse width to remain. This smoothened data is used as a resonable estimate of the baseline and is subtracted from the initial profile.

4.7 CONCLUSION

Using the observational and the data processing procedures described in this chapter attempts were made in the directions of more than 20 pulsars. The dispersion measures for these pulsars are in the range 12.4 to 79 $cm^{-3}pc$. An observing bandwidth(B) of 333 KHz was used in all cases. A sampling interval of 1.57 second was used. In the cases of only four pulsars, namely PSRs 0628-28, 0834+06, 0943+10 and 1919+21, was it possible to satisfy the detection criterion. For these pulsars, average pulse profiles were obtained with good sensitivity. As the values of Δf for three out of the four pulsars are larger than 333 KHz, it was possible to improve the time-resolution beyond (P/256) in these cases. The results obtained have amply demonstrated the ability of the scheme employed, to detect highly dispersed pulsar signals with high time-resolution. Fig. 4.14 shows one of the profiles obtained on PSR 1919+21.

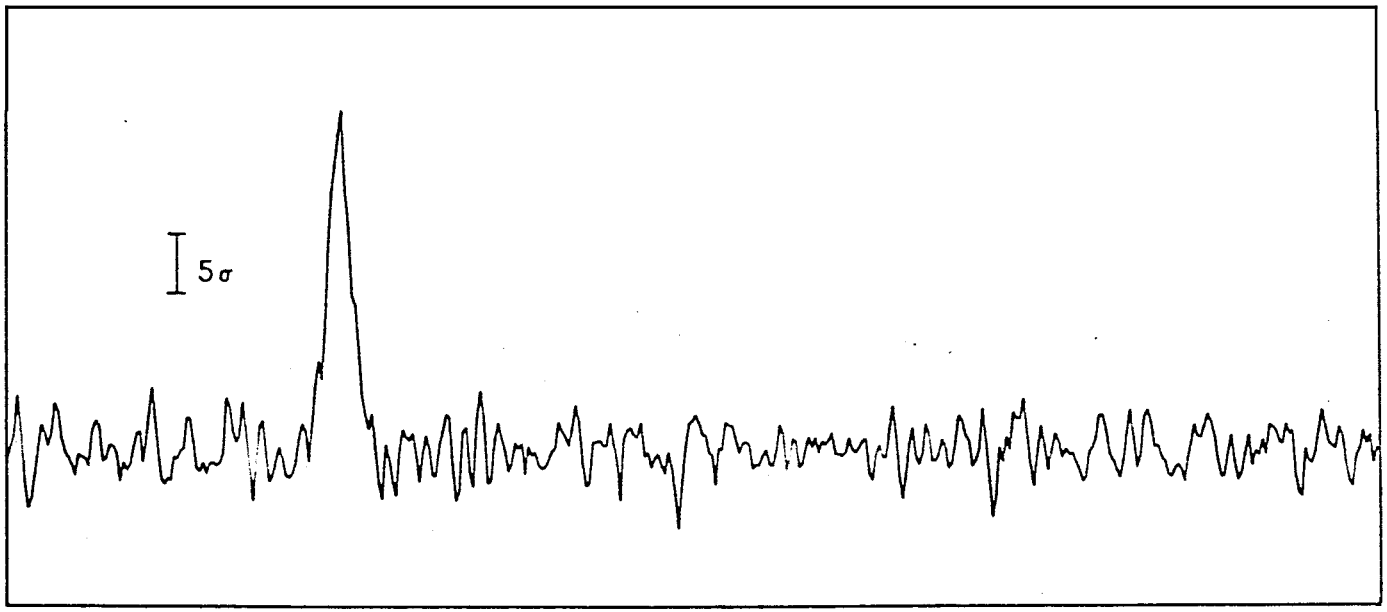

FIG.4.14 AVERAGE PROFILE OF PSR 1919+21 USING THE SWEPT-FREQUENCY DEDISPERSION SCHEME